Linear and nonlinear optical properties of sol-gel-derived Au nanometer-particle-doped alumina

Yousuke Hosoya and Taiji Suga
Faculty of Engineering, Tohoku University, Aramaki, Aoba-ku, Sendai 980-77, Japan

Tsutomu Yanagawa
NTT Opt-electronics Laboratories, 3-1 Morinosato Wakamiya, Atsugi, Kanagawa 243-01, Japan

Youichi Kurokawa[a)]
Faculty of Engineering, Tohoku University, Aramaki, Aoba-ku, Sendai 980-77, Japan

(Received 16 July 1996; accepted for publication 18 October 1996)

The precursor Au-doped alumina gel film was prepared by a sol-gel method using $HAuCl_4 \cdot 4H_2O$ and alumina sol derived from $AlCl_3 \cdot 6H_2O$. The precursor gel was heat treated in a H_2 gas flow at 300–800 °C. Average particle diameters of the Au particle of doped films were in the range of 4.6–12.7 nm. In the absorption spectra of the film, plasmon resonance absorption was strongly dependent on the heat treatment temperature of the alumina matrix, showing more sharp spectra and significant red shift with decreasing particle size. It was interpreted by a modified Mie–Drude equation by taking into consideration of a spilling out of electrons from the Au particle to the alumina matrix. The measured values of $\chi_m^{(3)}$ of the doped films are in the range of 9.2×10^{-6}–4.0×10^{-5} esu in the neighborhood of plasmon resonance wavelength of 530–570 nm. These are larger than those reported for the other doped systems. A dominant nonlinear response on the 1–3 ps time scale was obtained, reflecting higher thermoconductivity of alumina compared to that of conventional matrix such as SiO_2. © *1997 American Institute of Physics.* [S0021-8979(97)01403-5]

I. INTRODUCTION

The nanometer-sized noble metallic particles give rise not only to the change of color but also to optical enhancements in absorption, Raman scattering, and luminescence effects. Much attention has been paid to the study of optical properties of nanometer-sized particles dispersed in glass and polymer matrices from the viewpoint of scientific interest and their applications to nonlinear optical devices.[1–4] Hache *et al.* reported the enhanced third-order susceptibilities of colored filter glass.[5] Some reports on nonlinear optical (NLO) properties of noble metal particles have appeared during recent years.[6–13] The metal-particle-doped films are generally prepared by sputtering, ion implantation, sol-gel, and fusing methods. On the other hand, experiments for NLO properties of Au-particle-doped alumina film are rarely found in the literature. It seems that alumina is superior to silica in thermal conductivity and transmittance. The sol-gel method has been actively investigated as a new preparation method of glass at lower temperature; however, many works on this preparation are concerned exclusively with the silicate glass. We have reported a method to produce alumina film from inorganic salt.[14] Alumina film made from inorganic salt is more amorphous than that derived from alkoxide and can accommodate more amounts of dopants than those from aluminum and silica alkoxides.

II. EXPERIMENT

Alumina sol was prepared in a similar way to that previously reported.[14] Dropwise addition of aqueous NH_3 solution to aqueous $AlCl_3 \cdot 6H_2O$ solution brings about the precipitation of white polynucleic aluminum hydroxide. It was continued until reaching to *p*H 6.7. Then, the suspension solution was allowed to stand for about 12 h. If the standing period is not adequate, it becomes difficult to filter the precipitate after the standing and also impossible to peptize the precipitation at the next step after the filtration step. After 12 h standing, the white precipitate was filtered and washed with pure water. Acetic acid was added to the filtered-off precipitate and then the precipitate was heated at 80 °C for 8 h under stirring. In this step, peptization of the precipitate occurred and it was transformed unto a transparent alumina sol. The amount of acetic acid added was 0.15 mol per 1 mol of Al. If the amount is below this ratio, the peptization does not proceed easily. If the amount is beyond, white aluminum salt is produced after gellation. Aqueous $HAuCl_4$ solution was mixed with the resultant transparent sol. The mixture was poured on a flat plate such as polystyrene petri dish. It was then converted into an alumina gel film doped with $HAuCl_4$ by dehydration in an atmosphere at room temperature. This doped alumina film was then heated in H_2 gas in a reaction silica tube until reaching to the desired temperature (300–800 °C). In the process of raising temperature, acetic acid added for peptization is decomposed. Then the film was heated for 2 h at the established temperature under H_2 flow. Absorption spectra were recorded by a Shimadzu UV-2200 spectrophotometer. X-ray diffraction (XRD) was measured using Cu $K\alpha$ radiation with a Ni filter (40 kV, 30 mA) by a JEOL JXD-8SD XRL meter. The Crystal diameter and its distribution were measured by a Hitachi H-8010 transmission electron microscope (TEM). For TEM measurement, samples were prepared by mounting a piece of doped film on

a)Author to whom correspondence should be addressed.

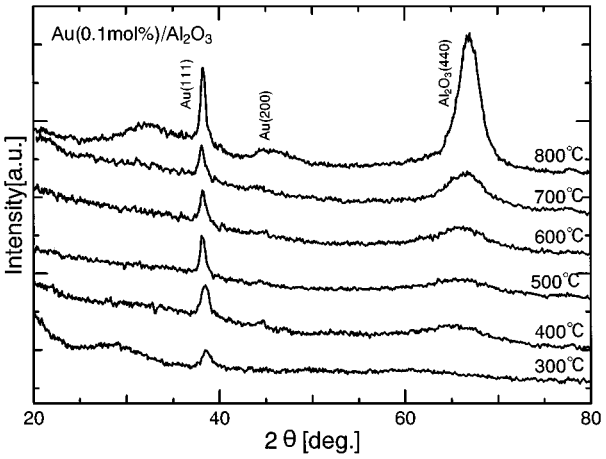

FIG. 1. X-ray-diffraction patterns of Au-particle-doped alumina films (0.1 mol %) treated at various temperatures.

a 200 mesh copper TEM grid. The mounted grids used the TEM operating at 150 kV. Particle size distributions were evaluated by measuring the diameters of particles on a photographically enlarged micrograph.

The third-order nonlinearities were determined using degenerate four-wave mixing (DFWM). The main part of the experimental setup has been described elsewhere.[15] DFWM was performed at different wavelengths (530, 550, and 570 nm) using a 10 Hz repetition rate. The pulse duration was about 8 ns for all wavelengths. The energy relaxation time T_1 of plasmon absorption was measured by using optical parameric oscillator (OPO) incoherent spectroscopy using the three-beam boxcar configuration.[16,17] It utilizes nanosecond optical pulses from an OPO that has a broad bandwidth and an ability of 100 fs response.[16]

III. RESULTS AND DISCUSSION

The resultant film is transparent and shows the color of red to violet which depends on the treatment temperature. Figure 1 shows the XRD patterns of the doped films. The peak, which can be clearly attributed to the (111) plane of the cubic structure of Au, appears on the diffraction pattern of amorphous alumina matrix. As increasing treatment temperature, the peak of the Au(111) plane becomes sharper and γ-Al_2O_3(440) develops at 700–800 °C. One can prepare the doped alumina film of desired thickness (0.1–100 μm) and of desired dopant concentration (0–0.5 mol % for alumina).

TABLE I. Mean particle size and physical properties of Au particle in alumina films treated at various temperatures.

Treated temperature (°C)	300	400	500	600	700	800
Average particle size $2R$ (nm)	4.6	5.0	8.8	10.0	11.9	12.8
Standard deviation	3.6	2.8	3.6	5.6	4.6	4.1
Plasmon frequency ω_p $[(s^{-1})\times 10^{15}]$	1.70	1.74	1.78	1.82	1.85	1.95
Electron density n_e $[(cm^{-3})\times 10^{22}]$	3.58	3.76	3.98	4.11	4.25	4.72

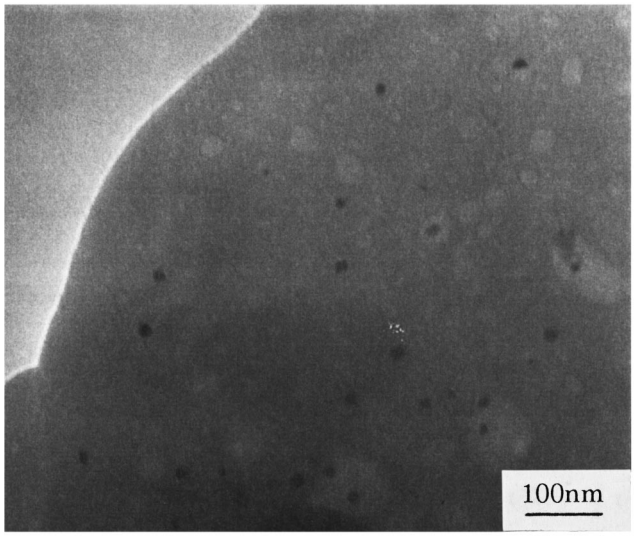

FIG. 2. TEM of Au particle-doped alumina film treated at 600 °C.

Here, the doped films used have about 50 μm thickness and contain 0.1 mol % Au for alumina. The amount of dopant into this amorphous alumina is one order of magnitude larger than that of conventional silica glass matrix. Figure 2 illustrates typical TEM image. They show the particles to be approximately spherical in shape and uniformly dispersed; however, a few larger particles, up to 2–3 times mean size, are detected. The sizes depend on treatment temperature of doped film. The mean sizes and standard deviations of the Au particle are shown in Table I. The mean sizes are in the range of 4.6–12.8 nm and increase with increasing treatment temperature of doped gel film, which agrees well with those determined from Scherrer's equation for XRD results. The size distributions evaluated by measuring the sizes of 300 particles on an enlarged micrograph are given in Fig. 3. These distributions become broad with increasing treatment temperature. It seems that the distributions reflect somewhat the densification of alumina matrix with increasing temperature. As shown in Fig. 3, the size distribution shifts to larger and broader size with increasing temperature. The precursor Au species, being insoluble in alumina itself, are contained

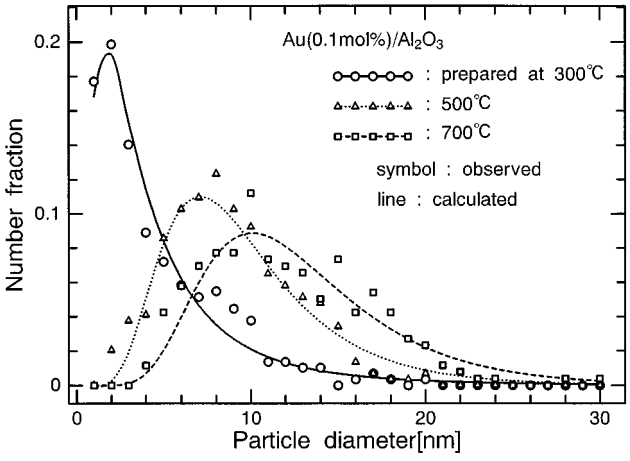

FIG. 3. Particle size distributions of Au particles in films. Doped films are the same as shown in Fig. 1.

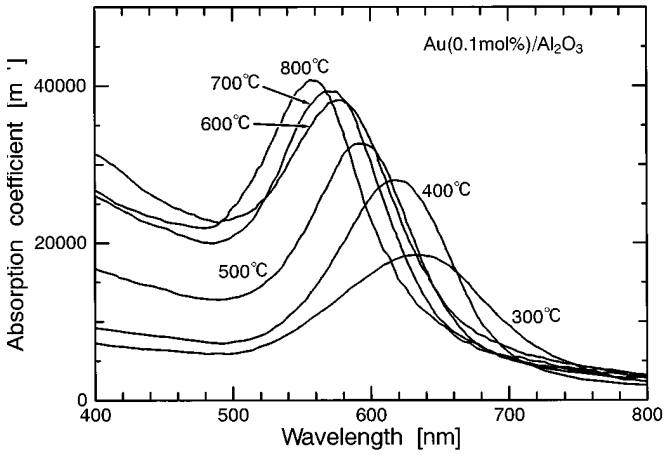

FIG. 4. Observed plasmon spectra of Au-particle-doped alumina films treated at various temperatures.

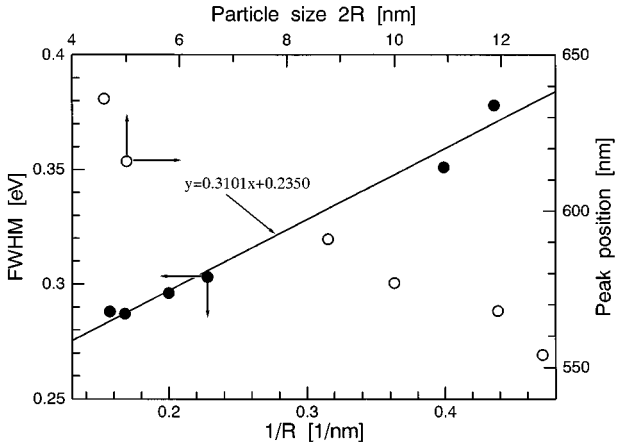

FIG. 5. Full width at half-maximum and peak position of plasmon spectra for Au-particle-doped alumina films.

in hydrophilic water domain distributed throughout the gel film, just as in the case of water inverse microemulsion. These salt-containing domains act as centers for nucleaction and growth of the particle. At the initial period of heat treatment, dehydration of the matrix occurs and $AuCl_4^-$ is densified. Then, at about 250 °C $AuCl_4^-$ is reduced by H_2 gas and nucleation occurs. Further heating causes dehydration and densification of the matrix, and nuclei contact each other to form the Au particle just like pore growing. Densification of wet gel to compact gel accompanies the elimination of H_2O from OH groups on the amorphous gel. This yields the microporosity of the gel. On increasing treatment temperature the pore size shifts to a larger and broader size by accompanying the decrease of pore volume.[14] Therefore, the particle growth and matrix transformation progress simultaneously. Assuming a process in which particle growing proceeds through two-particle conjugation, a simple distribution function called the ''log-normal'' distribution function (LNDF) can be statistically derived.[18] The resultant distribution function is

$$f_{\mathrm{LN}}(r)=\frac{1}{(2\pi)^{1/2}\ln\sigma_{\mathrm{LN}}}\exp\left[-\frac{1}{2}\left(\frac{\ln(r/\overline{r_{\mathrm{LN}}})}{\ln\sigma_{\mathrm{LN}}}\right)^2\right],$$

$$\sigma_{\mathrm{LN}}=\exp\left[\left(\frac{\Sigma_i n_i(\ln r_i-\ln\overline{r_{\mathrm{LN}}})^2}{\Sigma_i n_i}\right)^{1/2}\right], \tag{1}$$

$$\overline{r_{\mathrm{LN}}}=\exp\left(\frac{\Sigma_i n_i \ln r_i}{\Sigma_i n_i}\right).$$

Here r is the particle size. Calculated curves are in fair agreement with the observed distributions as shown in Fig. 3. It means that the particle formation may proceed inhomogeneously in microscopic scale just as is the case in the cluster-ion-beam method. This sol-gel reaction does not proceed in a fused state but does at a temperature (<800 °C) much lower than melting point (205 °C) of bulk alumina.

The absorption spectra of doped films are shown in Fig. 4. It shows only a single peak, indicating that the particles are uniformly distributed through the film and small enough in an application of the electrostatic approximation. The spectra broadens and the peak shifts to longer wavelength (red shift) as the particle size decreases. This behavior is opposite to that observed in the case of Au-particle-doped silicate glass.[19,20] This shift is also into the opposite direction from one predicted by a Mie–Drude equation described below. Figure 5 shows a size dependence of peak position, and a dependence of full width of half-maximum of peak on the inverse particle size which is commonly used in discussing the spectra by Hövel *et al.*[20] It has been known that the slope, being unity in an idealized system, turns out to be strongly influenced by the kind of matrix in a way that can-

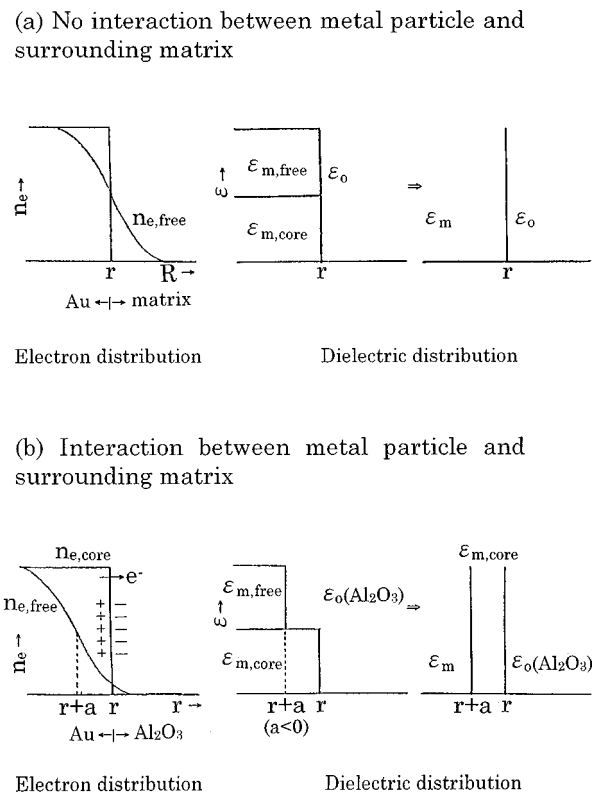

FIG. 6. Schematic representation of the two-region model for Au-particle-doped alumina film.

not be explained only by the dielectric property of the matrix.[19,20] The size dependence of peak has been the subject of a number of articles.[21–24] In the case of a noble metal particle, both blue and red shifts have been reported. The classical Mie theory, using the Drude expression for the dielectric function of particle, can be well applied to the particle dispersed system.[20] In the Mie equation the absorption cross section is

$$\sigma_{\mathrm{abs}}(\omega)=9k\epsilon_0^{3/2}V_0\,\frac{\epsilon_{m2}(\omega)}{[\epsilon_{m1}(\omega)+2\epsilon_0(\omega)]^2+\epsilon_{m2}(\omega)^2}, \quad (2)$$

where k and V_0 are the wave vector and particle volume, ϵ_0 and ϵ_m $(=\epsilon_{m1}+i\epsilon_{m2})$ are the dielectric functions of the matrix and metal particle, respectively. The Drude expression is

$$\epsilon_{m,\mathrm{free}}=1-\frac{\omega_p^2}{\omega^2-i(\omega/\tau)}, \quad (3)$$

where τ is a relaxation time and ω_p is the plasma frequency. It assumes that the metal contains free electrons which move restrictively by the positive lattice. The Mie–Drude prediction taking into account the dielectric constants of the bulk metal and of the matrix has been applied to explain the plasmon absorption peak. A common way to fit experimental data with the Mie equation is by the introduction of a size-dependent electron relaxation time in terms of the scattering at the surface; however, it cannot explain the large blue shift or size dependence of peak width evident in Fig. 4. The Mie–Drude expression yields the following plasmon frequency:[19,21]

$$\omega_M=\frac{\omega_p}{\sqrt{\epsilon_b+2\epsilon_0}}, \quad (4)$$

where ϵ_b is the dielectric constant of bound electron. The dielectric constant of alumina ϵ_0 is not changed significantly by treatment at 300–800 °C. The ω_p is given as

$$\omega_p=\left(\frac{4\pi n_e e^2}{m_e}\right)^{1/2}, \quad (5)$$

where n_e and m_e are the density and mass of electron, respectively. The ω_p and n_e obtained from fitting with the observed spectra are given in Table I. Namely, the free electron density decreases with decreasing particle size. The density profile is not modeled only by the particle size, form, or dielectric constants, but by the details of the surface surrounding particle. That is, physisorption, chemisorption, or another chemical interface interaction may induce the change of the electron density profile. In an aqueous sol, surface interactions including charge transfer to or from the particle have proved to change the peak width strongly.[19] In metal–alumina ceramic adhesion, two main interactions O–M and Al–M are found to be responsible for the adhesion strength of the interface.[25] The former interaction is repulsive, while the latter is attractive. To stabilize the adhesion energy, the electron transfers into a dangling bond on Al. There are many dangling bonds in the alumina of the metal–alumina interface that can accommodate electrons from the metal. In our ''amorphous'' alumina (as shown in Fig. 1) many dangling bonds can exist in matrix. On the other hand, it is reported that the direction of shift (red or blue) can be explained by taking into account the spill-out or -in of the free electron through the particle surface, affected by the matrix.[21–24] This gives the microscopic description for the two-region (core-shell) model in which the particle is approximated as containing an inner core region characterized by bulklike core dielectric functions and an outer shell region where the core polarization is ineffective.[22] When the free electron transfers from the particle to the matrix, the density of the free electron is reduced, then the dielectric function of the free electron can be regarded as having been missed in an outer region near the particle surface. It reduces the electron density and thereby the resonance frequency. Equation (2) is modified to Eq. (6) based on a two-region model, similar to the case of Ag particles embedded in a rare gas matrix,[22]

$$\sigma=9k\epsilon_0^{1/2}V_0\ \mathrm{Im}\left(\frac{(\epsilon_{m,\mathrm{free}}-\epsilon_0)(\epsilon_m+2\epsilon_{m,\mathrm{free}})+f(\epsilon_m-\epsilon_{m,\mathrm{free}})(\epsilon_0+2\epsilon_{m,\mathrm{free}})}{(\epsilon_{m,\mathrm{free}}+2\epsilon_0)(\epsilon_m+2\epsilon_{m,\mathrm{free}})-f(\epsilon_m-\epsilon_{m,\mathrm{free}})(2\epsilon_0-2\epsilon_{m,\mathrm{free}})}\right), \quad f=\left(\frac{r}{r+a}\right), \quad (6)$$

where a is the thickness of outer region. The outer region is a sort of mixing layer of particle surface with dangling bond of alumina. This layer corresponds to an adhesion boundary layer in adhesion of ceramic with metal.

The peak broadening is due to the spatial spreading and scattering of the electron across the particle–matrix interface.[25] The range of scattering (which is a measure of polarizability) is treated by adding or subtracting a spill-out distance to the particle size. In this theory, the free electron which contributes to plasmon absorption and is spilled out into the matrix is relaxated in its energy by the surrounding matrix before being scattered and returned into core particle. Figure 5 gives a slope of 0.31 which is comparable to that of the Ag particle doped in argon which is an inert matrix.[20] On the other hand, 1.4 is given for the Au/SiO_2 system. The slope 0.3 means that the contributing electron is hardly relaxated by the matrix on incident light, thereby electron damping is less and a narrower peak is yielded. Figure 6 illustrates the schematic figure of the Au/Al_2O_3 system by two-region model. In the outer region the free electron density is reduced by transfer into the matrix. The contributing free electron no longer reaches the surface and cannot be

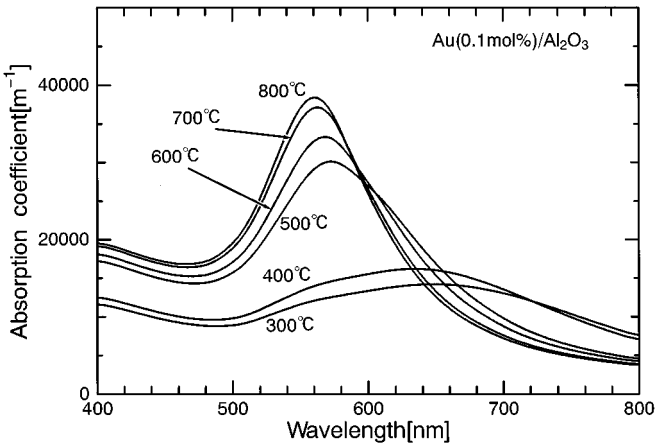

FIG. 7. Simulated plasmon spectra of Au-particle-doped alumina films by using the two-region model.

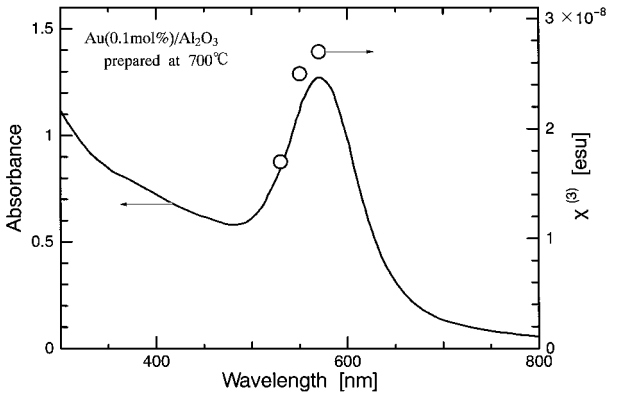

FIG. 8. $X^{(3)}$ values at near plasmon spectra of Au-particle-doped alumina film treated at 700 °C.

relaxed by the matrix, which causes the small slope value, 0.3.

In the calculation of the absorption spectra using Eq. (6) the peak shift depended on the thickness of the outer region. The thicker the outer region becomes, the larger the blue shift obtained. We have taken a mean value as a representative diameter for calculation. The calculated spectra using $a=-0.5$ nm for the thickness of the outer region are shown in Fig. 7, which is in fair agreement with Fig. 4.

In 1986 Hache and co-workers reported the third-order susceptibilities of colored filter glass which exhibited an enhancement by local field effects compared to bulk Au.[5] The susceptibilities of the Au/Al_2O_3 system were investigated by DFWM in the plasmon resonance region. The experimental results are given in Table II. The enhancement of local field inside the particle can take place at the plasmon resonance. A resonance enhancement is observed in the vicinity of the plasmon as illustrated typically in Fig. 8. The electric field inside the particle E_1 is related to the applied field E by

$$E_1=\frac{3\epsilon_0}{\epsilon_m+2\epsilon_0}E_0=f_1E_0. \tag{7}$$

f_1 is the local field factor given by the resonance enhancement.[5] The apparent nonlinear susceptibility $\chi^{(3)}$ is written by using the susceptibility $\chi_m^{(3)}$ which describes the nonlinear response to the local field E_1,

$$\chi^{(3)}=p|f_1|^2f_1^2\chi_m^{(3)}, \tag{8}$$

where p is the volume fraction of particle. In Table II f_1 and $\chi_m^{(3)}$ obtained from Eqs. (7) and (8) are listed. The observed $\chi_m^{(3)}$ is in the range of $0.5–2.3\times10^{-5}$ esu. These values are about two orders of magnitude larger than the reported values of $10^{-8}–10^{-7}$ esu for the aqueous Au colloid,[7] 10^{-8} esu for the Au glass system,[5] and 10^{-7} esu for the $Au/BaTiO_3$ system[12,13] and polymer.[25,26] On the other hand, it is reported that Au/SiO_2 glass prepared from sol-gel method gives a value of 2.6×10^{-6} esu.[27] It is thought that the large $\chi_m^{(3)}$ is due to the nonequilibrium state of the sol-gel-derived Au-doped SiO_2, since equilibrium is obtained by treating the doped SiO_2 at about 1000 °C.[27] In this doped alumina film the simultaneous formation of the alumina network and Au particle prevents the doped alumina from reaching the ther-

TABLE II. Photoproperties of Au-particle-doped alumina films.

	Treated temperature (°C)	Wavelength of measurement		
		530 nm	550 nm	570 nm
$\chi^{(3)}$ (esu)	300	1.3×10^{-8}	2.0×10^{-8}	3.0×10^{-8}
	700	1.7×10^{-8}	2.5×10^{-8}	2.7×10^{-8}
	800	1.3×10^{-8}	1.3×10^{-8}	1.3×10^{-8}
f_1	300	1.23	1.27	1.22
	700	1.78	1.82	1.65
	800	1.83	1.86	1.68
$\chi_m^{(3)}$ (esu)	300	1.7×10^{-5}	2.3×10^{-5}	4.0×10^{-5}
	700	5.0×10^{-6}	6.7×10^{-6}	1.1×10^{-5}
	800	9.2×10^{-6}	1.1×10^{-5}	2.8×10^{-5}
$\chi^{(3)}/\alpha$ (esu cm)	300	5.1×10^{-11}	5.9×10^{-11}	7.0×10^{-11}
	700	3.2×10^{-11}	3.5×10^{-11}	3.4×10^{-11}
	800	6.3×10^{-11}	6.7×10^{-11}	9.7×10^{-11}
T_1 (ps)	300	⋯	2.5	⋯
	700	⋯	1.1	⋯
	800	⋯	1.9	⋯

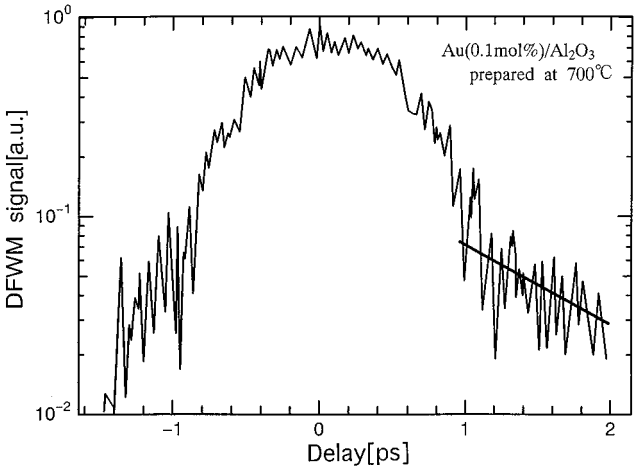

FIG. 9. Signal decay curve for the incoherent spectroscopy for Au-particle-doped alumina film treated at 700 °C.

TABLE III. Comparison of efficiency indicator for Au-doped system.

System	Au/H_2O[a]	Au/SiO_2[b]	Au/Al_2O_3
$\chi^{(3)}/(\alpha\tau)$ (esu cm s^{-1})	0.01–0.2	~2	~50

[a]Calculation from data in Ref. 7. It depends on particle size.
[b]Calculation from data in Ref. 28. It depends on response time in the range of <50 ps.

modynamic equilibrium. It can be considered that the electron transfer of the Au particle to the surrounding alumina matrix affects the electronic properties of the doped film and can contribute to an enhancement of $\chi_m^{(3)}$ because $\chi_m^{(3)}$ is calculated by using local field f. However, the errors from uncertainties of dielectric model, size distribution, etc., are incorporated in calculation of $\chi_m^{(3)}$. The susceptibility divided by α, $\chi^{(3)}/\alpha$ (α: absorption coefficient) is shown in Table II. Three mechanisms have been proposed to interpret the origins of $\chi_m^{(3)}$ for noble metal particles: hot electron and interband and intraband transitions.[5] The former two effects have been shown to be size independent. Only the intraband transition can explain the size dependence of $\chi_m^{(3)}$. The theoretical model predicts $\chi_m^{(3)}$ to be proportional to a reverse of the third power of particle size. Hache *et al.* have reported that the $\chi_m^{(3)}$ of Au/SiO_2 glasses with size ranging from 2.8 to 30 nm were roughly independent of particle size and that the value was equal to 5×10^{-8} esu; however, the size dependence of $\chi_m^{(3)}$ was not clearly observed in this experimental range. If there is any size effect, it may be only a weak one. The susceptibility is proportional to the fourth power of the local field factor determined by Eq. (8), however, as can be seen from Table II, f_1 is not so significant through the resonance enhancement. We treated the resonance enhancement that is due to a local field effect which was simply derived from the modified Mie equation. The original theoretical model is based on an idealized dielectric system, but these Au/Al_2O_3 films are not so ideal as described before. A more sophisticated model may be needed to evaluate the enhancement.

The photodynamics of nonlinear optics is often understood through the measurement of energy relaxation time T_1. Here an incoherent light source is utilized in forward DFWM with the three-beam boxcar configuration.[17] The decay curve for the DFWM signal of the Au/Al_2O_3 film during a successive change of probe without background shows the relaxation time constant T_1.[17] In Fig. 9 the background is subtracted already. The relaxation time is obtained from the fitted straight line on the logarithm curve. The obtained T_1, 1–3 ps, are shown in the last column of Table III. This value is lower than the reported value of 5 ps for the Au/SiO_2 system.[28,29] There was no slower T_1 component in our experiment at all. The higher thermoconductivite matrix tends to show the faster response. The dynamic efficiency indicator $\chi^{(3)}/\alpha\tau$ is roughly compared in Table III. Au/Al_2O_3 gives a significant efficiency indicator. It is not clear why the doped film gives higher efficiencies. Some reasons may be considered. The electronic state of the Au particle in alumina may be significantly different from that of bulk as described in plasmon absorption spectra. Alumina has one order larger thermoconductivity which affects dynamic response than conventional matrices such as SiO_2. In many experiments on noble-metal-particle-doped matrices one observes a dramatic increase of the peak width and small shift of the plasmon peak as particle size decreases.[11] The Au/Al_2O_3 films, however, give a narrow peak width and large red shift with decreasing size. This behavior is the opposite trend to what would be predicted from the original Mie equation. This different behavior may be revealed in the different NLO properties of doped systems.

IV. CONCLUSION

Au-particle-doped alumina film has been prepared by a sol-gel method using inorganic salt as a starting material. The plasmon absorption peak showed broader peak width and shifts to higher wavelength with decreasing size. This was treated by a modified Mie equation in terms of a two-region model for the distribution of the dielectric constant through the particle. The large NLO susceptibility and short relaxation time of the film was achieved.

[1] S. C. Davis and K. J. Klabunde, Chem. Rev. **82**, 153 (1982).
[2] E. J. Heilweil and R. M. Hochstrasser, J. Chem. Phys. **28**, 4762 (1985).
[3] G. Schmid, Chem. Rev. **92**, 1709 (1992).
[4] R. Lamber, S. Wetjen, G. Schultz-Ekloff, and A. Baalmann, J. Phys. C **99**, 13 834 (1995).
[5] F. Hache, D. Ricard, and C. Flytzanis, J. Opt. Soc. Am. B **3**, 1647 (1986); F. Hache, D. Ricard, C. Flytzanis, and U. Kreibig, Appl. Phys. A **47**, 347 (1988).
[6] J. W. Haus, N. Kalyaniwalla, R. Inguva, M. Bloemer, and C. M. Bowden, J. Opt. Soc. Am. B **6**, 797 (1989).
[7] M. J. Bloemer, J. W. Haus, and P. R. Ashley, J. Opt. Soc. Am. B **7**, 790 (1990).
[8] T. Dutton, B. Van Wonterghew, S. Saltiel, N. V. Chestnoy, P. M. Rentzepis, T. P. Shen, and D. Rogovin, J. Phys. C **94**, 1100 (1990).
[9] J. Matsuoka, R. Mizutani, H. Nasu, and K. Kamiya, J. Ceram. Soc. Jpn. **100**, 599 (1992).
[10] H. Kozuka and S. Sakka, Chem. Mater. **5**, 222 (1993).
[11] T. Yazawa, K. Kadono, H. Tanaka, T. Sakaguchi, S. Tsubota, K. Kuraoka, M. Miya, and W. De-Xion, J. Non-Cryst. Solids **170**, 105 (1994).
[12] T. Kineri, M. Mori, T. Tandano, T. Sakaguchi, M. Miya, H. Wakabayashi, and T. Tsuchiya, J. Ceram. Soc. Jpn. **103**, 117 (1995).
[13] I. Tanahashi, Y. Manabe, T. Tohda, S. Sasaki, and A. Nakamura, J. Appl. Phys. **79**, 1244 (1996).
[14] Y. Kurokawa, Y. Kobayashi, and S. Nakata, Heterogeneous Chem. Rev. **1**, 309 (1994).
[15] R. K. Jain and R. C. Lind, J. Opt. Soc. Am. **73**, 647 (1983).
[16] T. Yanagawa, K. Naganuma, H. Kanbara, and T. Kaino, Opt. Lett. **21**, 318 (1996).
[17] N. Morita, T. Tokizaki, and T. Yajima, J. Opt. Soc. Am. B **4**, 1269 (1987).
[18] C. G. Granqvist and R. A. Buhrman, J. Appl. Phys. **47**, 2200 (1976).
[19] V. Kreibig and L. Genzel, Surf. Sci. **156**, 678 (1985).
[20] H. Hövel, S. Fritz, A. Hilger, V. Kreibig, and M. Vollmer, Phys. Rev. B **48**, 18 178 (1993).
[21] M. Xu and M. J. Dignam, J. Chem. Phys. **96**, 3370 (1992).
[22] S. Fedrigo, W. Harbich, and J. Buttet, Phys. Rev. B **47**, 10 706 (1993).
[23] J. Tiggesbäumker, L. Köller, K.-H. M.-Broel, and A. Liebsch, Phys. Rev. A **48**, R1749 (1993).
[24] V. V. Kresin, Phys. Rev. B **51**, 1844 (1995).
[25] P. Alemany, R. S. Boorse, J. M. Burlitch, and R. Hoffmann, J. Phys. C **97**, 8464 (1993).
[26] S. Ogawa, Y. Hayashi, N. Kobayashi, T. Tokizaki, and A. Nakamura, Jpn. J. Phys. **33**, L331 (1994).
[27] M. Mennig, M. Schmitt, T. Burkhart, U. Becker, and H. Schmidt, Proc. SPIE **2288**, 130 (1994).
[28] D. Ricard, P. Roussignol, and C. Flytzanis, Opt. Lett. **10**, 511 (1985).
[29] R. H. Magruder III, Li Yang, R. F. Haglund, Jr., C. W. White, L. Yang, R. Dorsinville, and R. R. Alfano, Appl. Phys. Lett. **62**, 1730 (1993).